Astron. Astrophys. 302, 290–300 (1995)

ASTRONOMY AND ASTROPHYSICS

Long-term dynamical evolution of the brightest bolides

T.J. Jopek[1], **P. Farinella**[2], **Ch. Froeschlé**[3], **and R. Gonczi**[4]

[1] Obserwatorium Astronomiczne Uniwersytetu A.Mickiewicza, Sloneczna 36, Pl-Poznan, Poland
[2] Gruppo di Meccanica Spaziale, Dipartimento di Matematica, Università di Pisa, Via Buonarroti 2, I-56127 Pisa, Italy
[3] Observatoire de la Côte d'Azur, Dept. Cassini, URA CNRS 1362, B.P. 229, F-06304 Nice, France
[4] Observatoire de la Côte d'Azur, Dept. Cerga, URA CNRS 1360, B.P. 229, F-06304 Nice, France

Received 12 December 1994 / Accepted 8 March 1995

Abstract. We have integrated backwards in time the orbits of 17 very bright bolides — including four associated with meteorite finds — over a time span of 1 Myr or more. The results show dynamical mechanisms and evolutionary patterns fairly similar to those recently found for near–Earth asteroids, including frequent solar collisions, the widespread influence of secular resonances, some cases of comet–like hyperbolic ejections by Jupiter, and others of "slow–track" evolution driven by random encounters with the inner planets. This suggests that the sources for km–sized NEAs and metre–sized meteoroids are probably the same, and that the two types of bodies just sample different parts of the size distribution of a population of interplanetary objects with common dynamical features. The results of our integrations appear also consistent with the idea that ordinary chondrites come from the inner part of the main asteroid belt.

Key words: celestial mechanics – meteors, meteoroids – minor planets

1. Introduction

In the last decade substantial progress has been done in understanding the long–term dynamical evolution of the small interplanetary bodies which can approach the Earth and the other inner planets. Mainly, this has been triggered by the availability of fast and cheap computers, by which numerical experiments have been carried out with *ad hoc* integration algorithms capable of dealing effectively (and accurately) with the strong interactions occurring during close encounters (see e.g. Milani et al. 1989; Farinella et al. 1993a; Levison & Duncan 1994; Froeschlé et al. 1995). But a significant role has also been played by developments on the theoretical side, in particular in understanding the complexities of mean motion and secular resonances and of their interactions (Yoshikawa 1987, 1989, 1990; Morbidelli & Henrard 1991; Knežević et al. 1991; Morbidelli 1993; Morbidelli & Moons 1993; Moons & Morbidelli 1995).

Thus recent studies on the orbital evolution of real near–Earth asteroids (NEAs) over millions of years have revealed a variety of unexpected connections and phenomena: for instance, it has been found that secular and mean motion resonances can frequently increase the orbital eccentricity to almost unity, thus resulting into Sun–grazing episodes and even solar collisions (Farinella et al. 1994); and that accessible dynamical *routes* do exist between NEA–type orbits and those typical of comets and meteoroid streams (such as P/Encke and the Taurids), implying that dynamics alone cannot distinguish in the near–Earth population between rocky, asteroidal objects and extinct or "dormant", volatile–rich cometary nuclei (Valsecchi et al. 1995). Moreover, whereas near–Earth objects form a quasi–stationary population with dynamical and collisional lifetimes ranging from $\approx 10^5$ to 10^8 yr, large stochastic fluctuations appear possible, owing to the disruption of sizeable main–belt asteroids close to the resonant zones in the orbital element space (Menichella et al. 1995). Thus the cratering rate on the Earth may vary in a considerable way over geological time.

As for the typical sizes of these bodies, until a few years ago they were limited to being larger than several hundred metres. Only recently the Spacewatch Survey (Rabinowitz 1993; Rabinowitz et al. 1993) has detected bodies in Earth–grazing orbits in the diameter range between about 10 and 100 m. Very little is known on the origin and long–term dynamics of this population of very small near–Earth objects. As for the origin, sources of debris such as the disintegration of comets and lunar crater ejecta have been proposed as an alternative to main–belt asteroid fragments — widely thought to represent an adequate source for the larger NEAs (Farinella et al. 1993b; Morbidelli et al. 1994; Menichella et al. 1995). These unconventional sources would be likely to leave some "imprinting" on the observed dynamics of their offspring (at least in a statistical sense, since individual chaotic orbits quickly "forget" their initial conditions). Thus the observation that most very small NEAs have orbits with semi-major axes close to 1 AU and small eccentricities has led Rabinowitz et al. (1993) and Rabinowitz (1994) to claim that they

Send offprint requests to: P. Farinella

Table 1. A catalogue of the 17 brightest bolides. Orbital elements are given in the 1950.0 heliocentric ecliptic reference frame system. T_0 moment of apparition of the bolide

Bolide	T_0 (*in UT*) y m d h m s	a AU	e	q AU	Peri deg	Node deg	Inc deg	Size m
1 Grazing	72 08 10 202900	1.661	0.390	1.0127	355.6	317.956	15.22	10.
2 EN041274	74 12 04 175636	1.980	0.76	0.471	282.0	251.78	2.3	7.1
3 PN40503	69 10 09 071639	2.02	0.64	0.722	73.0	16.0	12.6	2.6
4 EN170171	71 01 17 182000	2.35	0.62	0.901	321.0	116.75	2.71	2.2
5 PN39470	66 12 11 011200	2.11	0.71	0.613	265.1	259.0	0.8	2.0
6 EN070591	91 05 07 230358	2.428	0.619	0.9246	218.65	46.314	23.7	1.9
7 PN39121	65 12 27 082105	2.11	0.71	0.597	86.5	95.0	5.4	1.9
8 Příbram	59 04 07 193021	2.401	0.671	0.7894	241.75	17.110	10.48	1.8
9 EN010677	77 06 01 214600	1.8	0.75	0.455	286.0	71.01	1.5	1.4
10 EN100469	69 04 10 214430	2.32	0.60	0.934	35.1	200.561	6.77	1.3
11 PN39434	66 11 05 104111	0.71	0.43	0.405	196.7	42.0	3.4	1.3
12 MORB952	84 02 23 021600	1.93	0.73	0.515	97.6	153.18	8.4	1.2
13 PN40401	69 06 29 092513	3.8	0.76	0.907	221.3	97.0	13.1	1.1
14 EN140863	63 08 14 214834	3.01	0.67	1.006	190.31	141.192	35.1	1.0
15 LostCity	70 01 04 021400	1.66	0.417	0.967	161.0	283.0	12.0	-
16 Innisfree	77 02 06 021738	1.872	0.4732	0.986	177.97	316.80	12.27	-
17 Peekskill	92 10 09 234800	1.49	0.41	0.886	308.0	17.030	4.9	-

cannot have the same source as the larger members of the NEA population. Yet, the observational selection effects involved in the astronomical discovery of NEAs — as a function of both size and orbital elements — are very complex, and their collisional evolution may be both size– and orbit–dependent (Farinella & Davis 1994). Therefore, in our opinion, the issue about the existence of a genetically distinct population of small NEAs is still open.

In this context, it is important to recall that the population of small near–Earth objects is known not only from astronomical observations, leading to the discovery of new NEAs and comets through telescopic surveys, but also from the data on the interaction with the Earth's atmosphere of the solid bodies which happen to hit our planet: in other words, from observations of meteors (Ceplecha 1992, 1994). Even the largest meteoroids, or bolides, are only metres in size, i.e. two to three orders of magnitude smaller than the typical sizes of the NEAs and comets discovered until only a few years ago, and close to the small–size end of the population currently observed by Spacewatch. Since the selection effects involved in the observations of bright meteors (or bolides) are very different from those involved in the telescopic discovery of NEAs/comets, these data represent an independent sampling from the current population of small near–Earth objects. For many bright meteors fairly accurate orbital information is available, and therefore their (past) long–term dynamical evolution can be studied with the tools of modern celestial mechanics in the same way as for the astronomically observed objects.

With this motivation, we have decided to integrate numerically backward in time the orbits of the 17 brightest bolides ever observed — including the four ones associated to definite meteorite finds — for a time span of the order of 10^6 yr, long enough to detect subtle secular effects. Although these orbits are strongly chaotic — hence the outputs of integrations cannot be seen as reproducing the real history of the real meteoroids — this exercise allows us to identify the main evolutionary patterns and dynamical mechanisms at work and to assess whether there is any significant difference with respect to the behaviour of the larger NEAs (as it is currently understood). Since the integration of these bodies, which by definition are very close to the Earth at the starting time, involves a number of preliminary steps which are not straightforward, in Sect. 2 we describe in some detail the procedure we have adopted in this work. Section 3 will describe and comment the main results inferred from the integration outputs on the long–term dynamics of these bodies. Some conclusions and open problems will be outlined in Sect. 4.

2. Calculation of the initial conditions

In this section we describe the procedure by which the initial positions and velocities of the bolides have been calculated. A list of 14 bodies with estimated sizes exceeding 1 metre was provided to us by Ceplecha (1993); orbital elements and sizes were derived from photographic observations of the corresponding fireballs, with the exception of the 1972 daylight Earth–grazing fireball (no. 1 in the list), for which they were derived by infrared tracking. We added to this list three more bolides (Lost City, Innisfree and Peekskill, nos. 15 to 17), which are the only ones besides Příbram (no. 8) associated to known meteorite falls. The corresponding data were taken from McCrosky et al. (1971), Halliday et al. (1978) and Brown et al. (1994), respectively. Table 1 summarizes all our starting data, with a number of significant digits consistent with their expected accuracy (apart from the apparition times T_0, which may be wrong by at most a few minutes); errors in the orbital elements are caused by the limited accuracy of both the observations and the atmospheric models used to reconstruct the trajectory prior to atmospheric entry. In all cases, however, these errors are small enough that a qualitative dynamical study such as performed in this paper is meaningful.

To fulfil the requirements of our long–term integration software, the data reported in Table 1 had to be:

- complemented by the moment of perihelion passage;
- transformed into rectangular coordinates;
- integrated to a common initial epoch.

Table 2. Rectangular coordinates of 17 bolides in the 1950.0 heliocentric ecliptic reference frame. T_0 is the corresponding epoch in the Ephemeris or TDT Julian days. x, y, z are given in AU, $\dot{x}$,$\dot{y}$,$\dot{z}$ in AU/day

No	T_0	x	y	z	$\dot{x}$	$\dot{y}$	$\dot{z}$
1	2441540.3540	0.752686	-0.622726	-0.270068	0.013335	0.010868	0.010476
2	2442386.2482	0.307829	0.857957	0.372085	-0.019490	-0.007426	-0.003916
3	2440503.8037	0.958802	0.252232	0.109390	-0.014349	0.012076	0.009699
4	2440969.2644	-0.443353	0.806972	0.349974	-0.021320	-0.004548	-0.000885
5	2439470.5504	0.188577	0.890039	0.385999	-0.019759	-0.007486	-0.003518
6	2448384.4618	-0.696993	-0.669471	-0.290342	0.017565	-0.005160	-0.011376
7	2439121.8484	-0.085278	0.894259	0.387829	-0.016566	-0.013106	-0.003862
8	2436666.3131	-0.956823	-0.270221	-0.117192	0.014170	-0.013197	-0.009636
9	2443296.4075	-0.326624	-0.870762	-0.377639	0.018978	0.007652	0.002882
10	2440322.4064	-0.938502	-0.322968	-0.140067	0.011862	-0.017315	-0.004814
11	2439434.9457	0.731790	0.604506	0.262167	-0.006804	0.010449	0.005391
12	2445753.5951	-0.880078	0.408209	0.177035	0.004419	-0.019752	-0.005944
13	2440401.8930	0.123837	-0.925297	-0.401291	0.019845	0.010477	-0.000740
14	2438256.4091	0.789037	-0.582190	-0.252489	0.010051	0.018833	-0.005634
15	2440590.5935	-0.221071	0.878509	0.380999	-0.019977	-0.000658	-0.004929
16	2443180.5961	-0.718908	0.619362	0.268610	-0.014237	-0.011811	-0.009992
17	2448905.4923	0.953738	0.268014	0.116234	-0.000870	0.017528	0.009396

Table 3. Sensitivity of the initial coordinates (x and $\dot{x}$ only) of a number of bolide orbits when the integrations to the common epoch are performed by setting to zero the Earth's mass for different intervals of time starting from T_0

No	x	$\dot{x}$	x	$\dot{x}$	x	$\dot{x}$	x	$\dot{x}$
	5 days		10 days		25 days		50 days	
2	3.394	-0.00154	3.394	-0.00154	3.394	-0.00154	3.394	-0.00154
5	3.314	0.00299	3.315	0.00299	3.315	0.00299	3.315	0.00299
6	-1.575	0.00242	-1.569	0.00260	-1.566	0.00268	-1.565	0.00270
7	2.375	-0.00803	2.376	-0.00802	2.377	-0.00802	2.377	-0.00802
12	-0.754	0.01058	-0.750	0.01079	-0.748	0.01089	-0.747	0.01091
16	2.303	0.00232	2.307	0.00226	2.311	0.00222	2.312	0.00220

The first step is easily done by finding first the true anomaly ϑ of the bolide. Since by definition meteoroids collide with the Earth at one node of their orbits, we have

$\vartheta = -\omega$, if the meteor was observed at the ascending node,

$\vartheta = 180° - \omega$, if the meteor was observed at the descending node,

Here ω is the argument of perihelion of the observed orbit. The required time of perihelion passage T_p is then found by applying the well–known formulae for Keplerian motion:

$$\tan\left(\frac{E}{2}\right) = \sqrt{\frac{(1-e)}{(1+e)}}\,\tan\left(\frac{\vartheta}{2}\right),$$

$$M = E - e\sin E,$$

$$T_p = T_0 - \frac{M}{n},$$

where e is the eccentricity, E the eccentric anomaly, M the mean anomaly, n the mean motion and T_0 the observation time. The rectangular coordinates of the bolides were then calculated by means of the classical formulae of celestial mechanics. The corresponding results are collected in Table 2.

In the next step, the state vectors of all bolides in Table 2 have been brought to the same osculating epoch. For this purpose a 15th order Taylor-Stephenson integrator was used (see e.g. Sitarski 1979; Dybczyński & Jopek 1986). The dynamical model was the Newtonian N–body problem including all the nine planets and the Moon, with masses and initial conditions taken from the JPL DE102 Planetary Ephemeris (Newhall et al. 1983). The integration was performed in two steps: starting from the epoch JD 2440000.5 the movement of all planets has been integrated till the osculating epoch of the given bolide (as given in Table 2), then the bolide was included and the integration was continued back to the epoch JD 2440000.5. It has to be noted, however, that the elements as given in Table 1

Table 4. Sensitivity of the integration procedure described in Sect. 2 to the uncertainties in the initial coordinates. The Table shows the maximum differences between final coordinates of the test particles associated to each bolide (Δx, Δy, Δz in AU; $\Delta\dot{x}$, $\Delta\dot{y}$, $\Delta\dot{z}$ in AU/day)

No	Δx	Δy	Δz	$\Delta\dot{x}$	$\Delta\dot{y}$	$\Delta\dot{z}$
1	0.005	0.010	0.003	0.00015	0.00005	0.00002
2	0.001	0.006	0.000	0.00004	0.00000	0.00000
3	0.001	0.001	0.000	0.00000	0.00001	0.00000
4	0.002	0.008	0.001	0.00001	0.00002	0.00000
5	0.001	0.001	0.000	0.00000	0.00000	0.00000
6	0.019	0.091	0.033	0.00055	0.00019	0.00024
7	0.007	0.002	0.001	0.00003	0.00001	0.00000
8	0.021	0.008	0.002	0.00003	0.00008	0.00001
9	0.005	0.002	0.000	0.00002	0.00001	0.00000
10	0.001	0.001	0.000	0.00000	0.00001	0.00000
11	0.005	0.004	0.000	0.00026	0.00021	0.00000
12	0.059	0.124	0.012	0.00281	0.00030	0.00014
13	0.002	0.002	0.001	0.00001	0.00000	0.00000
14	0.022	0.008	0.005	0.00007	0.00003	0.00005
15	0.001	0.004	0.000	0.00002	0.00002	0.00000
16	0.007	0.017	0.004	0.00009	0.00005	0.00001
16	0.007	0.017	0.004	0.00009	0.00005	0.00001
17	0.098	0.054	0.007	0.00087	0.00066	0.00003

Table 5. Rectangular coordinates of the 17 bolids at the common epoch JD 2440000.5. Reference frame: barycentric, ecliptic 1950.0 (x, y, z in AU; $\dot{x}$, $\dot{y}$, $\dot{z}$ in AU/day)

No	x	y	z	$\dot{x}$	$\dot{y}$	$\dot{z}$
1	0.99829	-0.319546	0.11677	0.0078894	0.0172854	0.0049303
2	3.39388	-0.001022	0.12920	-0.0015439	0.0046280	-0.0001162
3	-0.24039	-3.203608	-0.67295	0.0056414	-0.0008439	-0.0005300
4	-1.98756	-2.698276	0.14162	0.0028266	-0.0065923	0.0000211
5	3.31482	-1.329691	0.04890	0.0029936	0.0041246	0.0000299
6	-1.56541	0.561903	0.69296	0.0027031	-0.0131903	-0.0049139
7	2.37730	1.343024	-0.23453	-0.0080158	0.0027486	0.0007325
8	1.22921	3.704785	0.59057	-0.0043489	0.0026040	0.0006875
9	-2.50021	1.043917	0.07090	-0.0066476	-0.0033480	0.0001362
10	0.27907	3.098413	-0.33305	-0.0070474	-0.0035432	0.0001002
11	-0.30559	-0.271610	0.00033	0.0231311	-0.0220323	-0.0018923
12	-0.74736	0.073964	0.03855	0.0109063	-0.0224335	0.0022679
13	-4.15948	0.583182	0.94435	0.0049796	-0.0057848	-0.0009797
14	-1.89040	-0.975800	1.36839	0.0106624	-0.0041272	-0.0024319
15	-1.44982	-1.276012	-0.36215	0.0034717	-0.0105013	0.0002156
16	2.31195	-1.340554	0.13047	0.0021973	0.0075146	0.0015172
17	1.15710	-0.854337	-0.04015	0.0127115	-0.0071667	-0.0009074

had been calculated by using pre–atmospheric velocities and radiant coordinates already corrected for the deflection of the bolide's trajectory due to the Earth's gravity, simply by assuming a geocentric hyperbolic orbit of the approaching meteoroid. As a consequence, the rectangular coordinates of Table 2 give the state vectors of the orbits as they would have been if the final encounter with the Earth had not occurred. To be consistent with this, the Earth must be excluded from the integration of each bolide orbit starting at the respective observation epoch, for a time long enough to account for the effective duration of the final Earth encounter — but not too long, lest the long–range Earth perturbations on the pre–encounter bolide orbit, and possibly also the occurrence of previous Earth encounters, would be discounted as well. Of course, the choice of the best compromise is somewhat arbitrary: after a series of test integrations, we concluded that excluding the Earth for a time of 50 days since the observation time is sufficient to eliminate the effects of the final encounter to an accuracy of the same order as the observational accuracy of the starting data. Table 3 presents the results of these tests in a number of different cases, by showing the x and $\dot{x}$ values resulting from integrations where the Earth was excluded for 5, 10, 25 and 50 days since the observation time T_0. It should be kept in mind that the procedure described above involves some approximation, since excluding the Earth from the integration is not exactly the same as applying the hyperbolic deflection correction.

Since the orbital elements listed in Table 1 certainly include considerable observational and model errors, we may wonder whether the results of the integration procedure described earlier are sensitive to any small change in the values of the initial orbital elements. To estimate the propagation of these uncertainties to our final values for the coordinates and velocities to be used later on as initial conditions for the long–term integrations, we carried out the entire procedure described above to bring the orbits to a common epoch not only for the "real" bolide orbits, but also for a set of 4×17 "fictitious" orbits whose starting coordinates were obtained by superimposing 4 times to those listed in Table 2 a random "noise" of $R \times 10^{-4}$ AU (for the positions) and $R \times 10^{-6}$ AU/day (for the velocity components), where

Table 6. Osculating elements of the 17 bolids at the common epoch JD 2440000.5. Reference frame: heliocentric, ecliptic 1950.0

No	T_p JD	q AU	e	Peri deg	Node deg	Incl deg
1	2439974.03816	1.012	0.390	95.1	220.6	15.7
2	2440421.62868	0.473	0.759	348.9	185.3	24.2
3	2439511.46533	0.721	0.640	285.4	162.9	11.8
4	2439608.91528	0.900	0.620	263.1	174.2	24.8
5	2439515.82456	0.613	0.710	342.3	182.0	23.6
6	2440128.30453	0.925	0.618	151.2	109.6	18.8
7	2440245.19521	0.596	0.710	13.5	166.9	24.5
8	2439420.18398	0.778	0.674	90.8	167.5	13.7
9	2439755.20837	0.455	0.750	180.3	176.4	23.0
10	2440349.09241	0.934	0.600	51.4	184.8	29.9
11	2440004.38142	0.405	0.430	64.6	173.7	21.0
12	2440029.13740	0.513	0.731	77.0	172.9	31.2
13	2440431.35175	0.909	0.760	164.0	151.5	28.1
14	2440206.68321	1.003	0.671	172.6	153.9	55.1
15	2439794.93298	0.967	0.417	236.1	210.3	23.7
16	2440371.81694	0.987	0.473	286.0	210.5	16.6
17	2440114.30680	0.887	0.410	149.4	175.5	18.8

R is a random number distributed uniformly between 0 and 1. Table 4 shows the maximum differences between the final coordinates of the test particles corresponding to each bolide derived from this testing procedure. In general, the sensitivity does not appear very strong: for most of the orbits the differences are of the order of 10^{-2} AU and 10^{-4} AU/day, i.e. much larger than the initial "noise", but small enough that the long–term integrations to be discussed in Sect. 3 can still be seen as representative for the real population of small bodies hitting the Earth. The largest instability appears to be associated with bodies nos. 6, 12 and 17.

The final results, under the form of both rectangular coordinates and osculating Keplerian elements for all the 17 bolides at a common osculating epoch, are gathered in Tables 5 and 6.

3. Long-term integrations and results

We have integrated numerically the orbits of the 17 bolides with the initial conditions listed in Table 5. The integrations were carried out with a Bulirsch–Stoer variable–stepsize integrator (Stoer & Bulirsch 1980) and a purely gravitational model of the Solar System containing all the planets from Venus to Neptune.

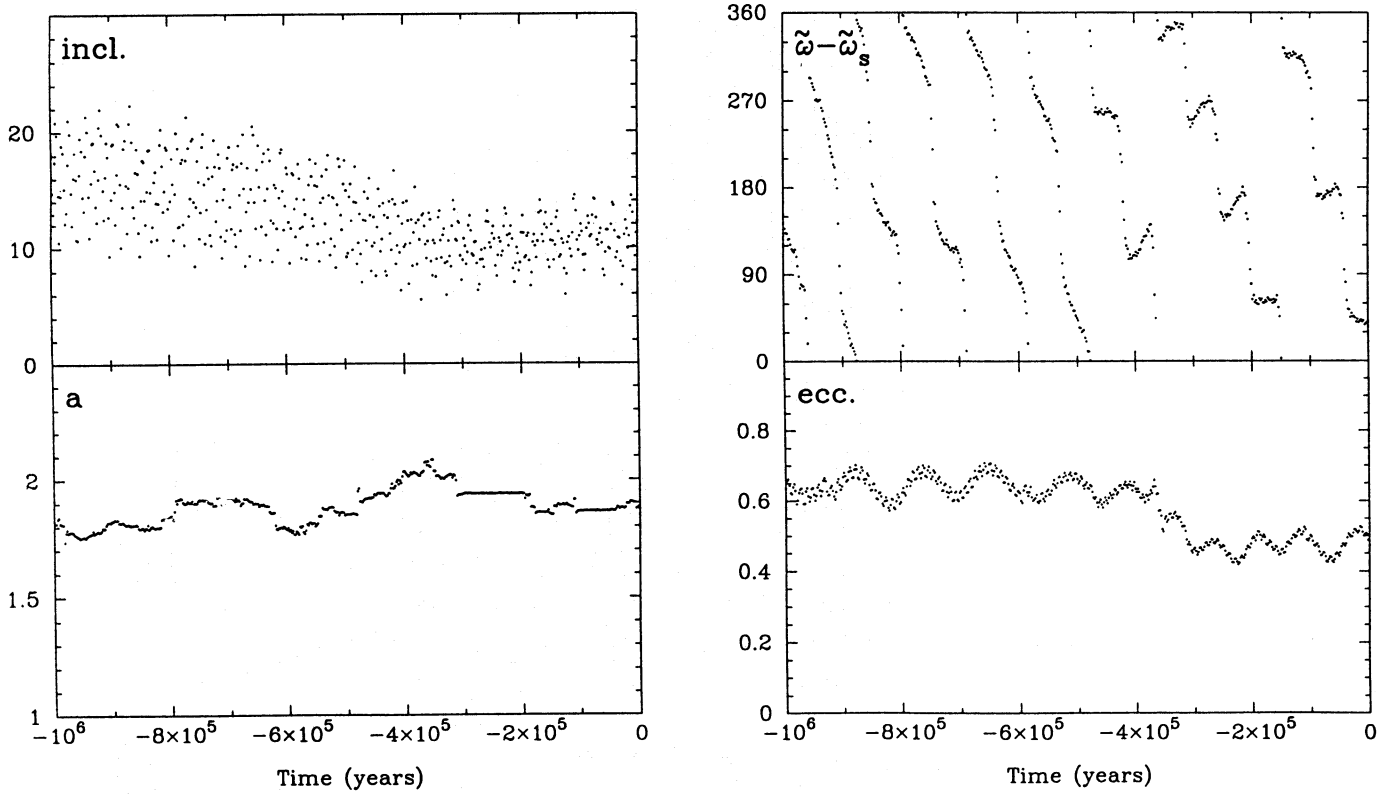

Fig. 1. Orbital evolution in the time span -1 Myr $< t < 0$ of bolide no. 16 (associated to the Innisfree meteorite fall). The figure shows the semimajor axis a (in AU), eccentricity e, inclination i (in degrees) and the critical argument $\varpi - \varpi_S$ of the ν_6 secular resonance (in degrees), versus time (in years). The slow circulation of $\varpi - \varpi_S$ implies that the body is rather close, but not inside the resonance

The integration time span extended from $t = 0$ (the common starting epoch JD 2440000.5) to $t = -1$ Myr in the past. As the orbits of these bodies are strongly chaotic, with Lyapounov exponential divergence times typically shorter than 10^3 yr, the results obtained from the numerical integrations cannot be seen as the real dynamical evolutions of the real meteoroids over time spans much longer than this. However, as discussed in several recent papers on the results of such long–term integrations (e.g. Levison & Duncan 1994; Farinella et al. 1994; Froeschlé et al. 1995), this kind of work is very useful to get qualitative and/or statistical information on the most frequent orbital behaviours and on the effectiveness of various dynamical mechanisms.

After having carefully looked at the the dynamical evolution of the 17 orbits, we think we can distinguish four kinds of basic behaviour:

3.1. Orbits dominated by close planetary approaches

Seven bodies (nos. 1, 2, 3, 5, 7, 16 and 17) have a dynamical evolution similar to that illustrated in Fig. 1. During the integration time, they get never locked into a secular or a mean motion resonance. Their semimajor axis just performs a sort of random walk due to frequent close approaches with the inner planets. The eccentricity and the inclination suffer moderate–amplitude oscillations of the order of 0.2 and 10°, respectively. The dynamical behaviour of these bodies is similar to that of the Geographos–class asteroids defined by Milani et al. (1989), or of the "slow–track" NEAs discussed by Froeschlé et al. (1995). Somewhat peculiar is the case of bolide no. 5, whose eccentricity stays always high and reaches a maximum value of about 0.95, whereas the inclination remains quite small ($0° \leq I \leq 5°$). The small inclination results into many close encounters with the inner planets which, however, are not very effective in changing the semimajor axis due to the high relative velocity between a very eccentric and a near–circular orbit. This behaviour resembles that of the Oljato–type NEAs as discussed by Milani et al. (1989).

3.2. Orbits falling into the Sun

In analogy with many NEAs whose orbital evolution has been studied by Farinella et al. (1994), the orbits of 5 bolides (nos. 4, 6, 9, 10 and 12) reach eccentrities very close to unity. As a consequence, their perihelion distance $q = a(1 - e)$ becomes smaller than $1\ R_\odot \approx 5 \times 10^{-3}$ AU, and a solar collision can be assumed to occur. All these bodies are temporarily in, or very close to, a secular resonance and/or a Jovian mean motion commensura-

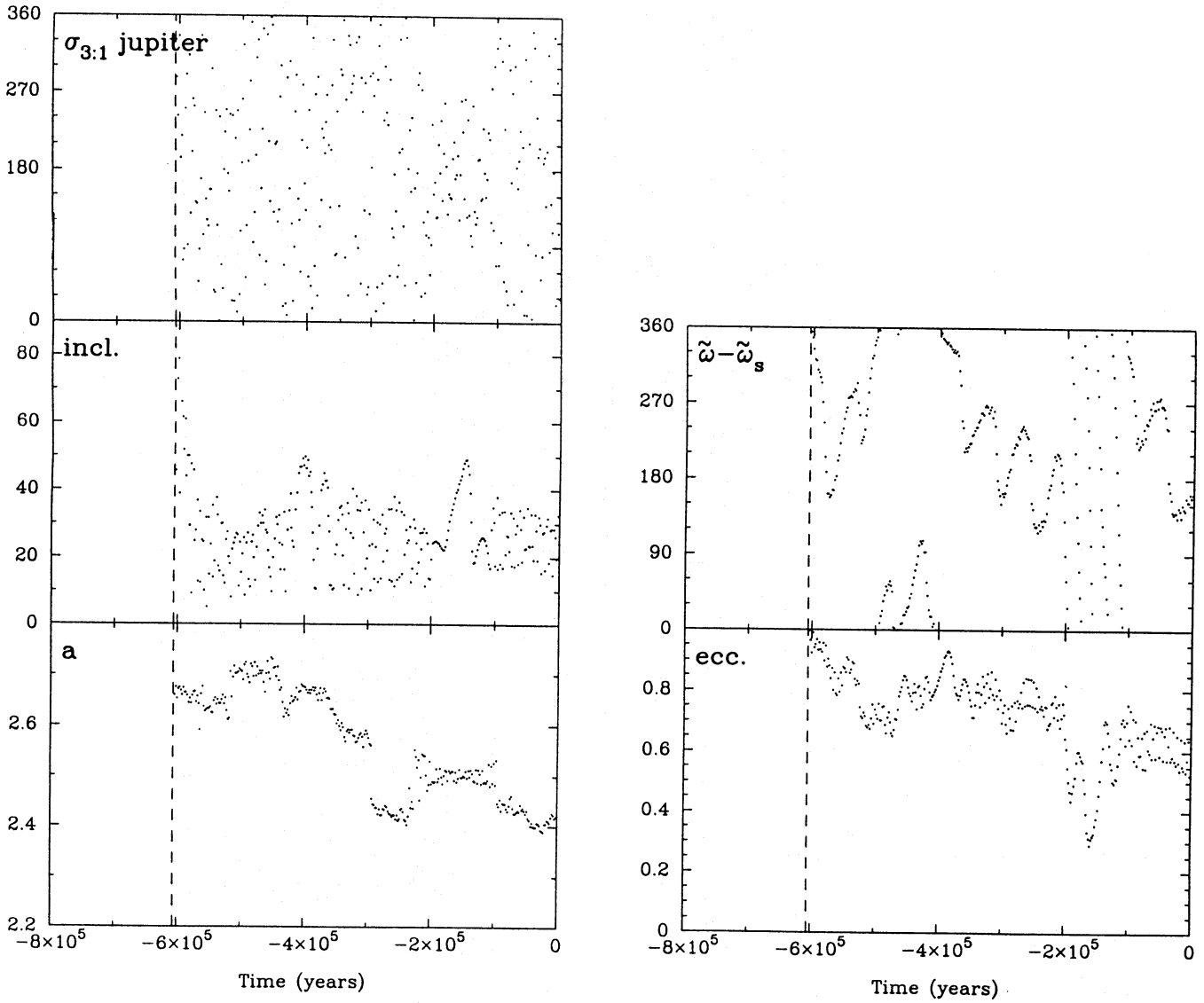

Fig. 2. Orbital evolution in the time span -0.8 Myr $< t < 0$ of bolide no. 6. The figure shows the semimajor axis a (in AU), eccentricity e, inclination i (in degrees) and the critical arguments of the ν_6 and 3:1 resonances (in degrees), versus time (in years)

bility. For instance, starting from $t = 0$ and going backward in time, bolide no. 6 stays in the ν_6 secular resonance until about $t = -10^5$ yr; then, a close planetary encounter injects it into the 3:1 mean motion commensurability with Jupiter, whence it is removed again by close encounters at about $t = -2 \times 10^5$ yr, ending up again in the ν_6 secular resonance (as shown by the libration around 0° of the critical argument $\varpi - \varpi_S$, i.e. the difference between the bolide's and Saturn's perihelion longitudes; see Fig. 2). The eccentricity is pumped to almost unity by the secular resonance, and the solar collision occurs at about $t = -6 \times 10^5$ yr. This mechanism has already been found by Farinella et al. (1994) to be effective for NEAs having starting values of the semimajor axis, eccentricity and inclination very close to those of this orbit. Also, it is well known that near $a \approx 2.4$ AU and at moderate inclinations, the ν_6 resonance is very effective in pumping up the eccentricity (Farinella et al. 1993a), so this object may well be a relatively recent newcomer from the main asteroid belt.

Another related mechanism, also described in Farinella et al. (1994), leads bolides nos. 4 and 10 to hit the Sun. These two bodies stay temporarily in the ν_6 secular resonance, but when are removed from it by close encounters, they have already such a high eccentricity value that subsequent moderate secular oscillations of the eccentricity are sufficient to cause a solar collision. Both these bolides fall into the Sun between $t = -6 \times 10^5$ yr and $t = -7 \times 10^5$ yr. A partially different case is that of bolide no. 9, which is never located inside a secular or a mean motion resonance. But it always stays close to ν_6, as shown by the fact that the $\varpi - \varpi_S$ critical argument circulates slowly (with a period of about 1.5×10^5 yr). The already high starting eccentricity value (0.75) increases secularly going back in the past, and reaches almost unity at about $t = -3 \times 10^5$ yr. Another variant is that of bolide no. 12 (see Fig. 3), which is

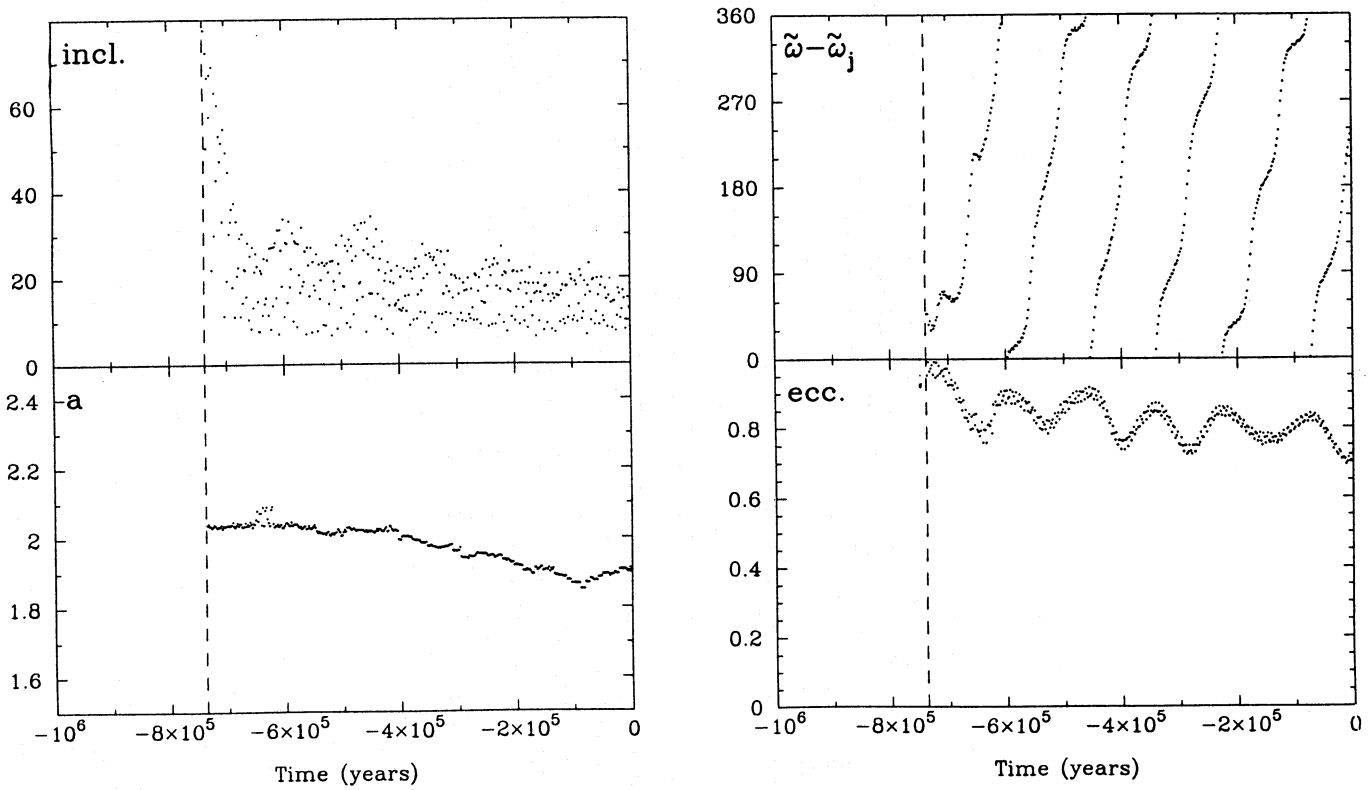

Fig. 3. Orbital evolution in the time span -1 Myr $< t < 0$ of bolide no. 12. The figure shows the semimajor axis a (in AU), eccentricity e, inclination i (in degrees) and the critical argument $\varpi - \varpi_J$ of the ν_5 secular resonance (in degrees), versus time (in years)

fairly close to the ν_5 resonance, with the circulation period of $\varpi - \varpi_J$ (the latter being Jupiter's perihelion longitude) of the order of 10^5 yr and the eccentricity reaching a peak every time that $\varpi - \varpi_J$ passes through 0°. These eccentricity oscillations (between about 0.7 and 0.9) last until (at about $t = -7 \times 10^5$ yr) the body enters the ν_5 secular resonance as a consequence of the encounter–driven drift in semimajor axis; this causes the eccentricity to rise quickly from 0.75 until unity, and consequently the body hits the Sun at $t = -7.4 \times 10^5$ yr.

3.3. Hyperbolic orbits

Bolides nos. 13 and 14 show a cometary–type orbital evolution in the past. Their aphelion distances at the time of observation (see Table 1) are such that close encounters with Jupiter can already happen near the beginning of the integrations. The orbit of bolide no. 13 becomes hyperbolic at $t = -1.5 \times 10^5$ yr. Bolide no. 14 (see Fig. 4) is in the ν_6 secular resonance during the whole integration time; it undergoes a first close encounter with Jupiter at about $t = -10^4$ yr, then for about 1.5×10^5 yr the eccentricity stays very high (up to about 0.95) and the inclination undergoes large oscillations (even exceeding 50°); at $t = -1.6 \times 10^5$ yr a sequence of strong encounters with Jupiter drastically increases the semimajor axis and the resulting comet–type orbit becomes hyperbolic at $t = -1.9 \times 10^5$ yr. Although this kind of behaviour is quite typical for short–period comets (Levison & Duncan 1994), it is also shared by a number of known NEAs (Milani et al. 1989; Farinella et al. 1994; Froeschlé et al. 1995). It is interesting to recall that, according to Ceplecha's (1988) analysis of the properties of thousands of sporadic meteoroids (see in particular his Fig. 3), some 20% among the largest of these bodies should be of cometary origin.

3.4. Temporarily resonant orbits

Bolide no. 8 stays in the ν_6 secular resonance until about $t = -2.5 \times 10^5$ yr (see Fig. 5). Before, the secular argument $\varpi - \varpi_S$ circulates slowly, the eccentricity is pumped up and down in a regular manner, with superimposed small oscillations of shorter period. In the interval -1 Myr $\leq t \leq -9 \times 10^5$ yr the body is in the 3:1 mean motion resonance, with large–amplitude oscillations in eccentricity and inclination. With time, this behaviour may well become strongly chaotic and lead to a solar collision (Farinella et al. 1994; Morbidelli & Moons 1995). As this bolide is associated to the Příbram meteorite fall, an H5 ordinary chondrite with a cosmic–ray exposure age between 20 and 40 Myr (Stauffer & Urey 1962; Fireman & DeFelice 1963; Lavrukhina et al. 1974), our results support the idea that

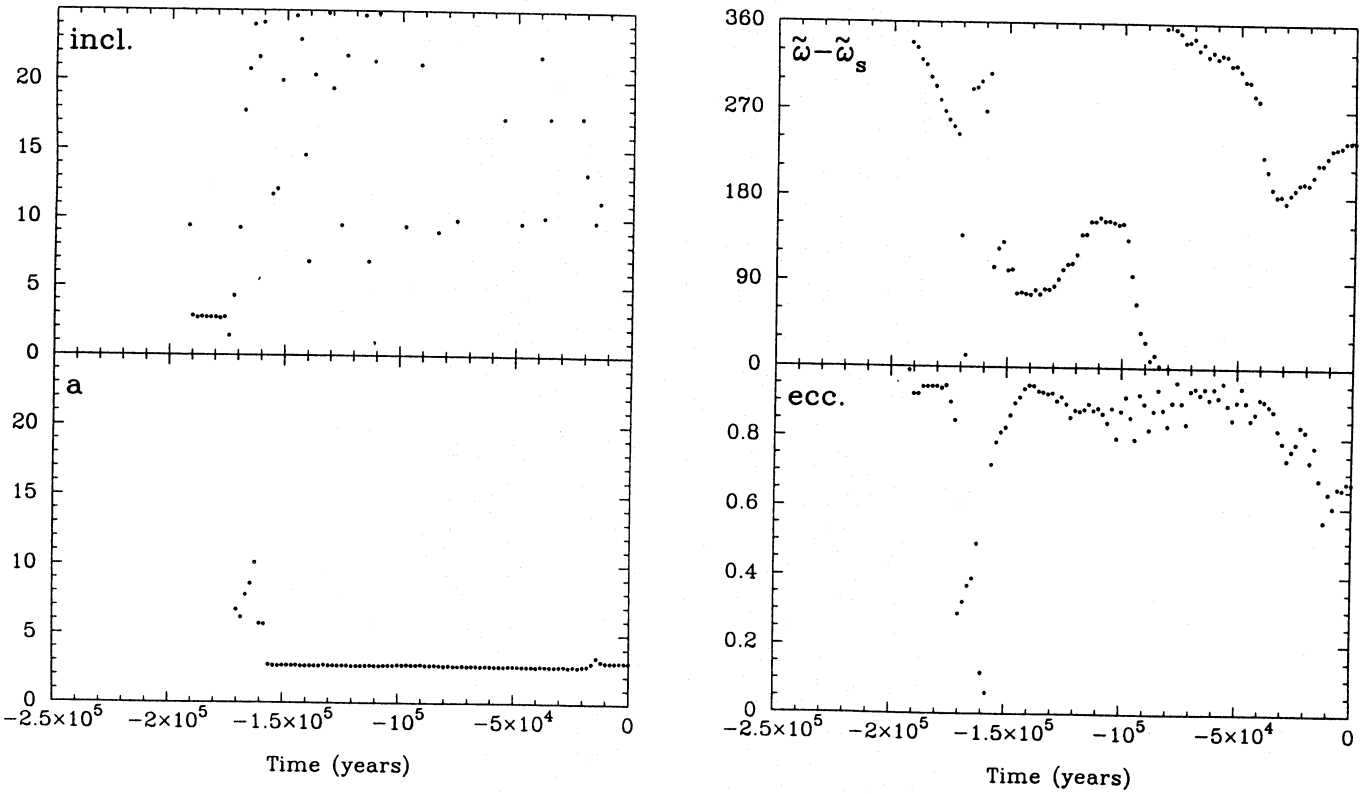

Fig. 4. Orbital evolution in the time span -0.25 Myr $< t < 0$ of bolide no. 14. The figure shows the semimajor axis a (in AU), eccentricity e, inclination i (in degrees) and the critical argument $\varpi - \varpi_S$ of the ν_6 secular resonance (in degrees), versus time (in years)

this meteorite came from the main asteroid belt through the ν_6 and/or 3:1 resonant *routes* (Farinella et al. 1993a).

Bolide 11 is an Aten–type object. For -2×10^5 yr $\leq t \leq 0$, it stays locked in the ν_5 secular resonance, despite the small inclination, showing no strong effect on the orbital elements. For the rest of the time, it behaves like a class 1 object, with semimajor axis changes dominated by encounters. As pointed out by Froeschlé et al. (1995), the dynamics in the region $a \leq 2$ AU is complicated by the direct secular effects of the terrestrial planets, and as a consequence the locations and effects of secular resonances are still largely unknown for this type of orbits.

In the case of bolide no. 15, we extended the integration until $t = -3$ Myr, to better understand the eventual outcome of the clear trends in eccentricity and semimajor axis (both of them increase going toward the past). During the interval -3 Myr $< t < 1.6$ Myr, the semimajor axis of this body is almost constant, with an eccentricity small enough (about 0.2) to prevent Earth encounters. Encounters with Mars are possible, albeit not very frequent; but due to the small mass of Mars, these encounters are not very effective in changing the semimajor axis (see Fig. 6). But eventually a Mars encounter increases the semimajor axis enough to inject the body in the ν_6 resonance at about $a = 2.05$ AU. In the interval $-1.6 \leq t \leq -1.3$ Myr, the resonance pumps up the eccentricity to about 0.6, and then Earth encounters become possible and the semimajor axis random–walks down to about 1.75 AU in a relatively fast manner. This example shows clearly that orbits of this type may evolve from the inner edge of main asteroid belt, when Mars encounters put them under the influence of the ν_6 secular resonance; subsequently, Earth encounters may result into a Geographos–type non–resonant orbit. This kind of mechanism was pointed out long ago as a possible *route* for meteorite transport (Wetherill & Williams 1979); to our knowledge, this is the first time a numerical experiment provides a specific demonstration of it. Although we stress again that numerical integrations cannot trace back in a deterministic way the source region of any individual body, it is intriguing to note that this same object is associated to the Lost City meteorite fall, an H5 ordinary chondrite, and that according to Wetherill & ReVelle (1981) many fainter fireballs have similar physical and orbital properties. Thus, like in the case of Příbram we discussed earlier, the results of this integration appear consistent with the idea that ordinary chondrites come from the inner part of the asteroid belt. As for the other two meteorites whose pre–fall orbits are known, Innisfree and Peekskill (our bolides nos. 16 and 17), by analogy with this case it is reasonable to assume that their current class 1 (encounter–dominated) orbits may have evolved from resonant ones over a time scale of several Myr.

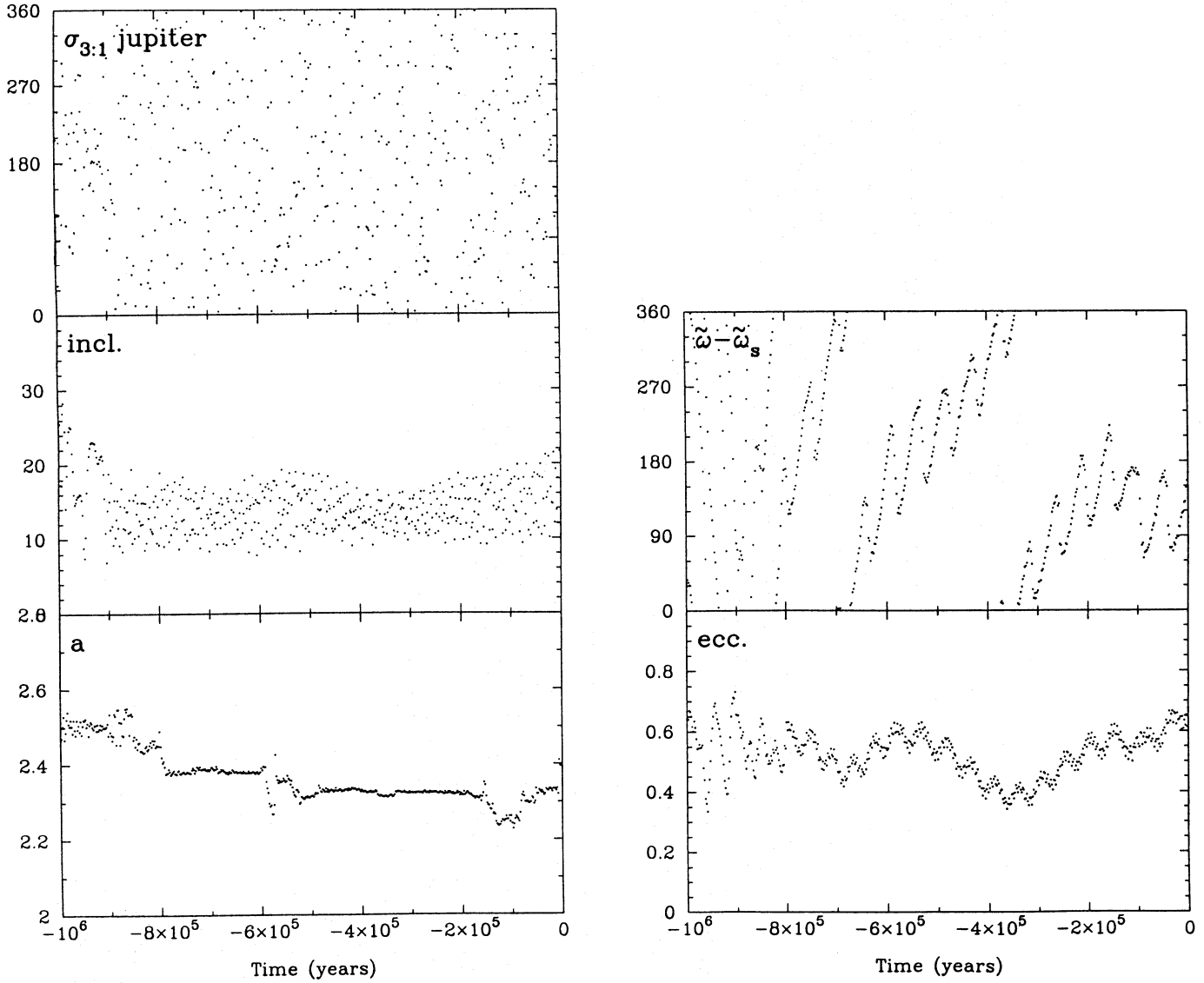

Fig. 5. Orbital evolution in the time span -1 Myr $< t < 0$ of bolide no. 8 (associated to the Příbram meteorite fall). The figure shows the semimajor axis a (in AU), eccentricity e, inclination i (in degrees), and the critical arguments of the ν_6 and 3:1 resonances (in degrees), versus time (in years)

4. Conclusions

The most interesting results from the work reported in this paper appear to be the following:

(1) We have developed a self–consistent procedure to carry out long–term numerical integrations of small interplanetary objects whose orbits had been derived by meteor data rather than telescopic observations. Although these orbits are by definition strongly chaotic (they end up hitting the Earth!) and this prevents us from tracing back the individual dynamical histories of the corresponding meteoroids, when such studies are performed over a large enough sample, valuable information can be derived on the most common dynamical mechanisms and evolutionary patterns.

(2) Despite the fact that the bodies whose dynamics has been studied here are two to three orders of magnitude smaller than typical NEAs, their long–term dynamical evolution appears strikingly similar to that of these larger bodies, as resulting from recent dynamical work (see in particular Farinella et al. 1994; Froeschlé et al. 1995). This similarity includes the crucial role of resonances (especially the ν_6 secular resonance) in causing drastic variations of eccentricity on time scales $< 10^6$ yr, the relatively high frequency of solar collisions, the existence of a minor fraction of comet–type orbits which end up into hyperbolic ejections by Jupiter, and the possibility that some objects settle on relatively long–lived, "slow–track" orbits affected by planetary encounters but not by resonances. It must be stressed that this similarity between the behaviour of meteoroids and NEAs is even more impressive when one considers that the

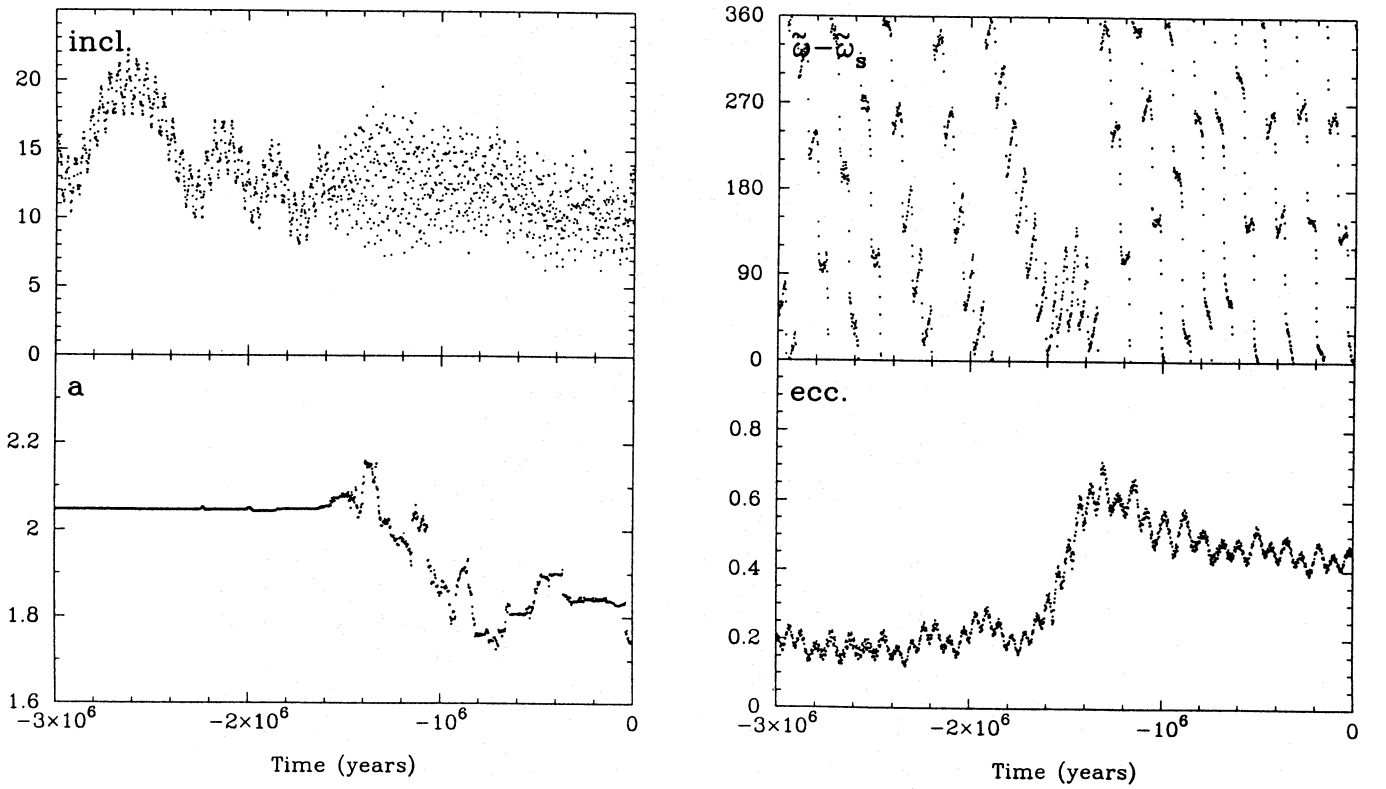

Fig. 6. Orbital evolution in the time span -3 Myr $< t < 0$ of bolide no. 15 (associated to the Lost City meteorite fall). The figure shows the semimajor axis a (in AU), eccentricity e, inclination i (in degrees) and the critical argument $\varpi - \varpi_S$ of the ν_6 secular resonance (in degrees), versus time (in years)

discovery selection effects and the criteria used to choose the samples of orbits to be integrated were completely different in the two cases. Although this kind of evidence cannot provide definite proofs on the origins and sources of the different populations of small interplanetary objects, in our opinion it gives a strong hint that the astronomically observed, km–sized NEAs and the metre–sized bolides just sample different parts of the size distribution of a dynamically homogeneous population. This appears at odds with the claim by Rabinowitz et al. (1993) and Rabinowitz (1994) that very small (10 to 100 m) NEAs have a peculiar distribution of orbital parameters, and would suggest that such a distribution is only an artifact of poor statistics and complex discovery selection effects.

(3) Since the "fast–track", rapidly evolving orbits account for about half of our sample, and since collisional lifetimes for metre–sized meteoroids probably exceed 1 Myr, our results suggest that a significant fraction of meteoroids were generated in the main asteroid belt fairly recently, and reached the Earth before suffering further disrupting collisions. On the other hand, the "slow–track" orbits may have remained parked in the planet–crossing region for much longer times (tens or even hundreds of Myr), so in this case much older typical ages would be implied. Qualitatively, such a variety of "dynamical ages" appears to be consistent with the evidence provided by the distribution of cosmic–ray exposure ages of ordinary chondrites, the most common meteorites (we recall that such exposure ages measure the time interval between the formation of a meteoroid as a metre–sized object and its eventual fall onto the Earth). This distribution is very broad, ranging from $\approx$ 1 to 100 Myr, with a clear peak at about 8 Myr for H–chondrites (Anders 1964; Crabb & Schultz 1981; Marti & Graf 1992). We suggest that this peak may mark the occurrence of a recent, relatively large–scale collision on a main–belt asteroid close in orbital element space to a resonance, as discussed by Farinella et al. (1993a), whereas the long–lived part of the distribution may consist of objects parked for a long time on a "slow track", for which collisional and dynamical lifetimes were of the same order.

(4) The existence of a minor fraction (2/17) of bolide orbits which since the very beginning of the integrations undergo close encounters with Jupiter and are then rapidly ejected from the Solar System suggests that metre–sized meteoroids of cometary origin are fairly common, albeit not the majority, in agreement with the conclusions of Ceplecha (1988, 1994) from a completely independent set of data. Again, this is fairly similar to

the current best guesses on the abundance of dormant/extinct cometary nuclei among NEAs (see e.g. Binzel et al. 1992).

(5) Our results for the four bolides associated with meteorite falls (in particular those for Lost City and Příbram), are fully consistent with the idea that the corresponding bodies have been transported by resonant mechanisms to Earth–crossing orbits from the inner part of the main asteroid belt. This strengthens the hypothesis that the parent bodies of ordinary chondrites are located in this region.

Acknowledgements. We are grateful to Z. Ceplecha for sending us the starting data on meteoroid orbits and for other helpful suggestions. We also thank the reviewer A. Milani for some useful remarks, as well as our colleagues D.R. Davis, C. Froeschlé, A. Morbidelli and G.B. Valsecchi for many discussions on related issues. P.F. carried out part of this work while staying at the Observatoire de la Côte d'Azur (Nice, France) thanks to the "G. Colombo" fellowship of the European Space Agency.

References

Anders, J.B., 1964, Space Sci. Rev. 3, 583
Binzel, R.P., Xu, S., Bus, S.J., Bowell, E., 1992, Science 257, 779
Brown, P., Ceplecha, Z., Hawkes, R.L. et al., 1994, Nature 367, 62
Ceplecha, Z., 1988, Bull. Astron. Inst. Czech. 39, 221
Ceplecha, Z., 1992, A&A 263, 361
Ceplecha, Z., 1993, private communication
Ceplecha, Z., 1994, in Asteroids, Comets, Meteors 1993 (A. Milani, M. Di Martino & A. Cellino, eds.), pp. 343–356, Kluwer, Dordrecht
Crabb, J., Schultz, L., 1981. Geochim. Cosmochim. Acta 45, 2151
Dybczyński, P.A., Jopek, T.J., 1986, Acta Astron. 36, 153
Farinella, P., Gonczi, R., Froeschlé, Ch., 1993a, Celest. Mech. 56, 287
Farinella, P., Gonczi, R., Froeschlé, Ch., Froeschlé, C., 1993b, Icarus 101, 174
Farinella, P., Davis, D.R., 1994, Bull. Amer. Astron. Soc. 26, 1167
Farinella, P., Froeschlé, Ch., Froeschlé, C. et al., 1994, Nature 371, 314
Fireman, E.L., DeFelice, J., 1964, Bull. Astron. Inst. Czech. 15, 113
Froeschlé, Ch., Farinella, P., Gonczi, R., Hahn, G., Morbidelli, A., 1995, Icarus, submitted
Halliday, I., Blackwell, A.T., Griffin, A.A., 1978, J. Roy. Soc. Canada, 72, 15
Knežević, Z., Milani, A., Farinella, P., Froeschlé, Ch., Froeschlé, C., 1991, Icarus 93, 316
Lavrukhina, A.K., Fisenko, A.V., Kolesnikov, E.M., 1974, Bull. Astron. Inst. Czech. 25, 122
Levison, H.F., Duncan, M.J., 1994, Icarus 108, 18
Marti, K., Graf, T., 1992. Annu. Rew. Earth Planet. Sci. 20, 221
McCrosky, R.E., Posen, A., Schwartz, G., Shao, C.-Y., 1971, J. Geophys. Res. 76, 4090
Menichella, M., Paolicchi, P., Farinella, P., 1995, Earth Moon & Planets, in press
Milani, A., Carpino, M., Hahn, G., Nobili, A.M., 1989, Icarus 78, 212
Moons, M., Morbidelli, A., 1995, Icarus 114, 33
Morbidelli, A., 1993, Icarus 105, 48
Morbidelli, A., Henrard, J., 1991, Celest. Mech. 51, 169
Morbidelli, A., Moons, M., 1993, Icarus 102, 316
Morbidelli, A., Moons, M., 1995, Icarus, submitted
Morbidelli, A., Gonczi, R., Froeschlé, Ch., Farinella, P., 1994, A&A 282, 955
Newhall, X.X., Standish, E.M. Jr., Williams, J.G., 1983, A&A 125, 150
Rabinowitz, D., 1993, Astrophys. J. 407, 412
Rabinowitz, D., 1994, Icarus 111, 364
Rabinowitz, D., Gehrels, T., Scotti, J.V. et al., 1993, Nature 363, 704
Sitarski, G., 1979, Acta Astron. 29, 401
Stauffer, H., Urey, H.C., 1962, Bull. Astron. Inst. Czech. 13, 106
Stoer, J., Bulirsch, R., 1980, Introduction to Numerical Analysis, Springer Verlag, New York
Valsecchi, G.B., Morbidelli, A., Gonczi, R., Farinella, P., Froeschlé, C., 1995, Icarus, submitted
Wetherill, G.W., Williams, J.G., 1979, In: L.H. Ahrens (ed.), Origin and Distribution of the Elements, Pergamon Press, Oxford, p. 19
Wetherill, G.W., ReVelle, D.O., 1981, Icarus 48, 308
Yoshikawa, M., 1987, Celest. Mech. 40, 233
Yoshikawa, M., 1989, A&A 213, 436
Yoshikawa, M., 1990, Icarus 87, 78

This article was processed by the author using Springer-Verlag LaTeX A&A style file version 3.